AMERICAN SOCIETY FOR MICROBIOLOGY | mBio®

RESEARCH ARTICLE

Regulator of Actin-Based Motility (RoaM) Downregulates Actin Tail Formation by *Rickettsia rickettsii* and Is Negatively Selected in Mammalian Cell Culture

Adam M. Nock,[a] Tina R. Clark,[a] Ted Hackstadt[a]

[a]Host-Parasite Interactions Section, Laboratory of Bacteriology, Rocky Mountain Laboratories, National Institute of Allergy and Infectious Diseases, National Institutes of Health, Hamilton, Montana, USA

ABSTRACT The etiological agent of Rocky Mountain spotted fever, *Rickettsia rickettsii*, is an obligately intracellular pathogen that induces the polymerization of actin filaments to propel the bacterium through the cytoplasm and spread to new host cells. Cell-to-cell spread via actin-based motility is considered a key virulence determinant for spotted fever group rickettsiae, as interruption of *sca2*, the gene directly responsible for actin polymerization, has been shown to reduce fever in guinea pigs. However, little is known about how, or if, motility is regulated by the bacterium itself. We isolated a hyperspreading variant of *R. rickettsii* Sheila Smith that produces actin tails at an increased rate. *A1G_06520* (*roaM* [regulator of actin-based motility]) was identified as a negative regulator of actin tail formation. Disruption of RoaM significantly increased the number of actin tails compared to the wild-type strain but did not increase virulence in guinea pigs; however, overexpression of RoaM dramatically decreased the presence of actin tails and moderated fever response. Localization experiments suggest that RoaM is not secreted, while reverse transcription-quantitative PCR (RT-qPCR) data show that various levels of RoaM do not significantly affect the expression of the known rickettsial actin-regulating proteins *sca2*, *sca4*, and *rickA*. Taken together, the data suggest a previously unrecognized level of regulation of actin-based motility in spotted fever group rickettsiae. Although this gene is intact in many isolates of spotted fever, transitional, and ancestral group *Rickettsia* spp., it is often ablated in highly passaged laboratory strains. Serial passage experiments revealed strong negative selection of *roaM* in Vero 76 cells.

IMPORTANCE The mechanism of actin-based motility of spotted fever group *Rickettsia* has been studied extensively, but here, we provide genetic evidence that motility is a regulated process in *R. rickettsii*. The findings also suggest that serial passage of rickettsial strains in cell culture may cause the bacteria to lose essential genes that are no longer conserved under natural selective pressure. These findings are likely relevant to the interpretation of studies concerning virulence determinants of rickettsiae.

KEYWORDS *Rickettsia*, actin, vector-borne diseases

Rickettsia rickettsii is an obligately intracellular pathogen that causes Rocky Mountain spotted fever, a disease with the highest mortality of any tick-borne rickettsial disease (1, 2). Although originally recognized during the early 1900s in the Bitterroot Valley of western Montana, it has since become clear that the highest incidence in the United States occurs in the south-central states (3, 4). In the last 2 decades, case numbers have also begun to rise in the southwestern United States and Mexico (5). Numbers of spotted fever rickettsiosis caused by other members of the genus have also risen, seemingly correlated with a rising coincidence of people and ticks, as different species of ticks increase their range and numbers (6, 7).

Editor Craig R. Roy, Yale University School of Medicine

Address correspondence to Ted Hackstadt, thackstadt@niaid.nih.gov.

The authors declare no conflict of interest.

This article is a direct contribution from Ted Hackstadt, a Fellow of the American Academy of Microbiology, who arranged for and secured reviews by Christopher Paddock, Centers for Disease Control and Prevention, and Kevin Macaluso, University of South Alabama College of Medicine.

Received 9 February 2022
Accepted 18 February 2022
Published 14 March 2022

Members of the spotted fever group of rickettsiae, including *R. rickettsii*, utilize the polymerization of host actin to generate long actin tails that propel the bacterium through the cytoplasm of the host cell (8, 9). Actin-based motility contributes to a bacterium's ability to infect adjacent cells and has been studied using several facultative intracellular bacteria as models, including *Listeria monocytogenes*, *Shigella flexneri*, and *Burkholderia pseudomallei* (10–12). For these model pathogens, impairing actin-based motility results in smaller plaque sizes in cell culture models (11, 13, 14) and typically attenuates virulence (15). The development of plaque assays for rickettsiae enabled characterization of strains based on different plaque phenotypes (16–19). Comparison of plaque phenotypes, especially within the same species, has allowed the unraveling of genetic factors that lead to those phenotypes (20, 21). Within the spotted fever group, a reduced plaque size led to recognition that Sca2 is responsible for actin-based motility, and its ablation leads to decreased virulence in the guinea pig model (20, 22, 23). However, neither plaque size (21, 24) nor opacity (21) alone is a reliable indicator of virulence.

Mutations in *roaM*, a gene of unknown function, were initially identified in comparative genomics studies of the genetic differences between virulent and avirulent *R. rickettsii* (25, 26). The avirulent Iowa strain has an M4I amino acid change compared to the virulent Morgan and Sheila Smith strains, while the Morgan strain contained a base pair insertion resulting in an approximately 20% truncation of the protein product. Further investigations of this gene in Sheila Smith revealed a point deletion in some, but not all, *R. rickettsii* Sheila Smith subclones. Upon inspection, the emergence of the point mutation in *roaM* correlated with the emergence of large, clear plaques in later passages of *R. rickettsii* Sheila Smith. Annotated spotted fever group rickettsia genomes indicated frequent truncation of *roaM* even within a single species. Further investigation revealed a rapid loss of *roaM* in mammalian cell culture, suggesting that it may be beneficial in the tick vector but selected against in cell culture. Therefore, we pursued the possible connection between *roaM* and actin-based motility as well as stability of wild-type *roaM* during mammalian cell passage.

RESULTS

The genotype of *roaM* in Sheila Smith derived strains correlates with different plaque phenotypes. The parental Sheila Smith small-plaque variant (SS_S) carries an intact *roaM* and displays a small plaque phenotype. To assess the significance of *roaM* and its potential relation to plaque size, we generated several strains of *R. rickettsii* Sheila Smith with various *roaM* genotypes (Fig. 1A). SS_S-pROAM-FL and SS_S-pROAM-T constitutively produce N-terminally FLAG-tagged full-length and truncated versions of RoaM, respectively (Fig. S1). A genetic knockout of *roaM* (SS_S-Δ*roaM*) was generated via plasmid-based homologous recombination (Fig. S2). Growth curves (Fig. 1B) show similar rates of growth of all *R. rickettsii* variants and mutants in the exponential phase between 0 and 2 days postinfection. Deletion or truncation of *roaM* resulted in larger plaque sizes at both 8 and 15 days postinfection compared to SS_S (Fig. 1C and D). The overexpression of full-length *roaM* resulted in reduced plaque size. Interestingly, overexpression of truncated *roaM* in SS_S (SS_S-pROAM-T) resulted in an intermediate phenotype, suggesting a dominant or perhaps competitive effect over wild-type RoaM. The chromosomal copy of *roaM* for SS_S-pROAM-T was PCR amplified and Sanger sequenced to rule out inadvertent recombination or truncation.

Infection of Vero cell monolayers reveals differential patterns of spread determined by *roaM* genotype. Infection at a low multiplicity of infection (MOI) of 0.1 results in distinctly small foci with limited cell-to-cell spread of rickettsiae at 24 h postinfection (hpi) for SS_S (Fig. 2A). Overexpression of *roaM* FL exacerbates these small foci. Comparatively, rickettsiae with truncated *roaM* or lacking *roaM* appear more evenly distributed throughout the monolayer. The average number of rickettsiae per cell was determined. SS_L, SS_S-Δ*roaM*, and SS_S-pROAM-T on average contained between 2 and 4 rickettsiae, while SS_S and SS_S-pROAM-FL contained between 4 and 5 rickettsiae, with a larger standard deviation (Fig. 2B). Images were also quantified for the ratio of infected cells to total cells, revealing

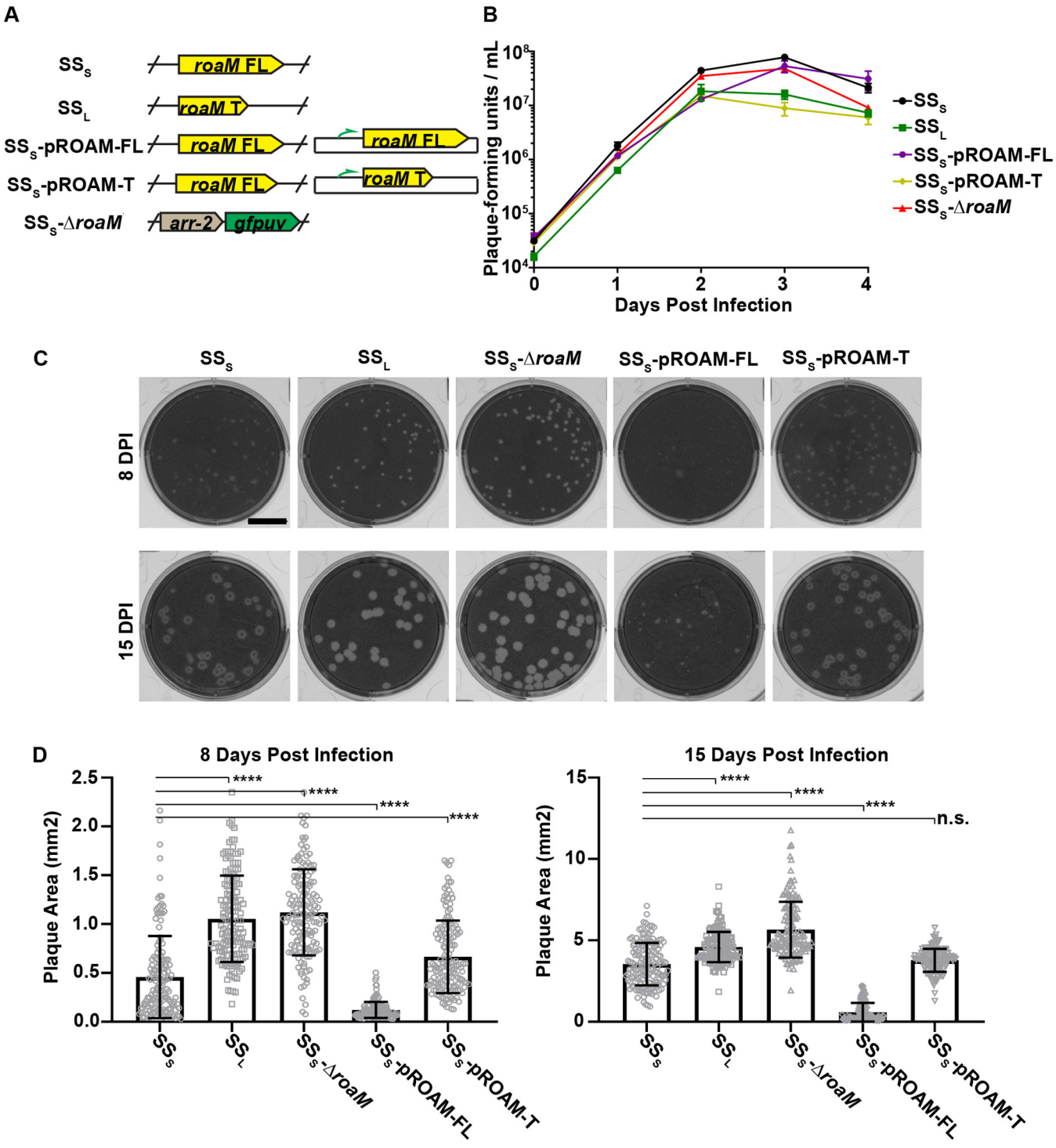

FIG 1 Differential *roaM* genotype in *R. rickettsii* Sheila Smith-derived strains results in varied plaque-size phenotypes. (A) Schematic of the genotype of critical strains used in this study. SS$_S$, Sheila Smith wild-type small-plaque variant; SS$_L$, Sheila Smith large-plaque variant; SS$_S$-pROAM-FL, SS$_S$ with ectopically expressed, full-length *roaM*; SS$_S$-pROAM-T, SS$_S$ with ectopically expressed truncated *roaM* producing a 211-amino-acid (aa) variant as found in SS$_L$; and SS$_S$-Δ*roaM*, SS$_S$ with a chromosomal deletion of *roaM*. (B) Growth curves for the above strains reveal no substantial difference in exponential growth rate. (C) Representative photographs of *R. rickettsii* plaques on six-well plates stained at either 8 or 15 days postinfection. Bar = 1 cm. (D) Pooled data from three independent experiments measuring plaque area, measuring 50 plaques per strain per experiment. Error bars represent standard deviations. Standard analysis of variance (ANOVA) followed by Tukey's multiple comparison was performed on results. ****, $P \leq 0.0001$; n.s., not significant.

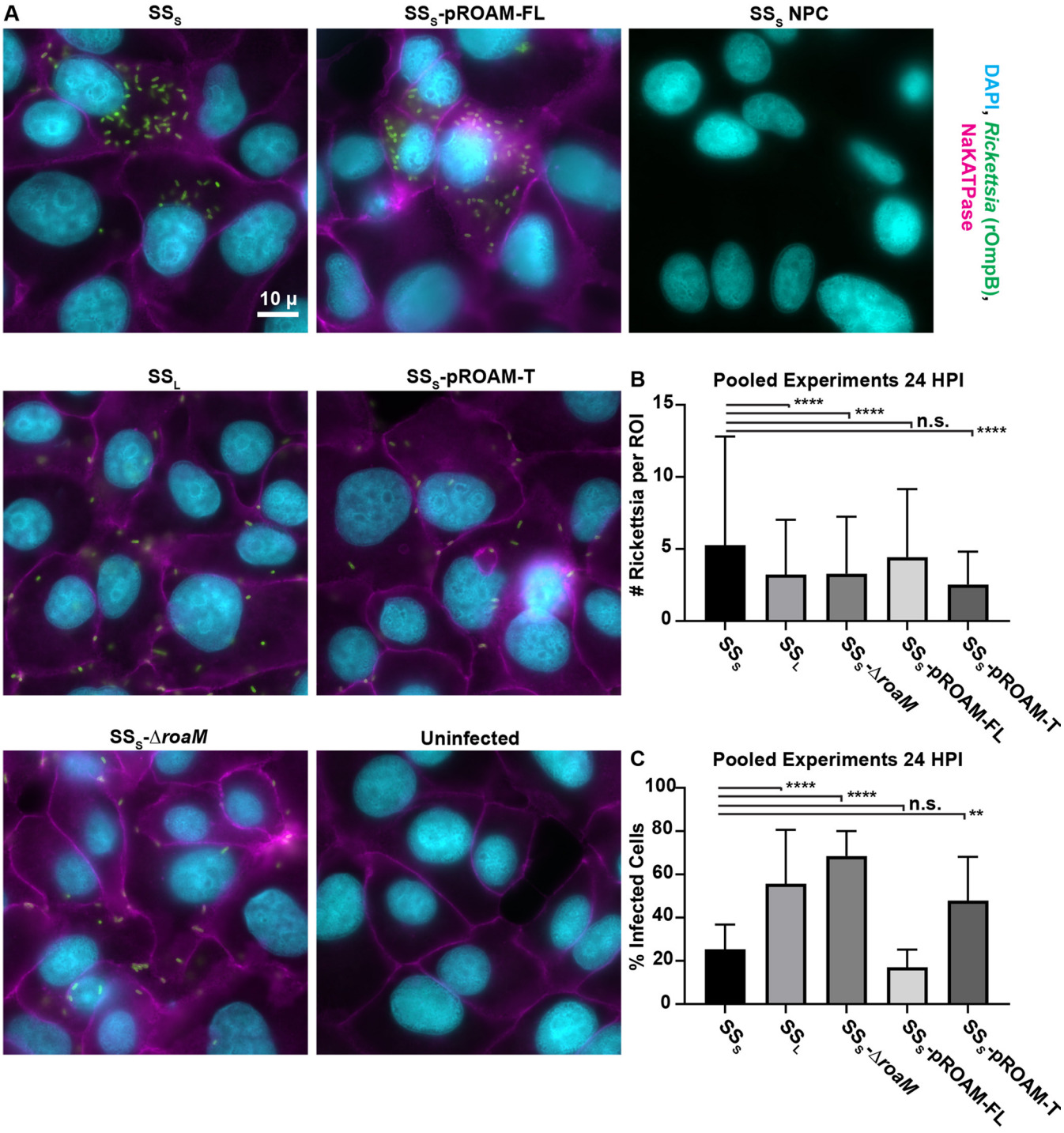

FIG 2 Low-MOI infection of Vero cells reveals differing rates of cell-to-cell spread among strains. (A) Vero cell monolayers on coverslips were infected at an MOI of 0.1, incubated at 34°C, and fixed with methanol at 24 or 48 h. An IFA was performed using anti-Na/K ATPase to visualize membrane boundaries (magenta), MAb 13-2 (66) for rickettsiae (green), and DAPI as a nuclear stain (cyan). Representative wide-field microscopy images are shown. The control with no primary antibody to rickettsiae (NPC) is a single, representative z-plane. Five randomly acquired wide-field images each from three independent infections for each strain were analyzed using Imaris 9.7 software by automated segmentation of nuclear and cell boundaries, as well as rickettsia identification. (B and C) Data from all experiments were pooled to show (B) the number of rickettsiae per ROI, with ROI representing single z-planes of individually segmented Vero cells at 24 h postinfection, and (C) the average percentage of infected cells per field. Error bars represent standard deviation. Statistics performed include standard ANOVA followed by Dunnett's multiple-comparison test. ****, $P \leq 0.0001$; **, $P = 0.0014$; n.s., not significant.

that infection with SS_L, SS_S-Δ*roaM*, and SS_S-pROAM-T led to more frequent cell-to-cell spread with a resultant higher percentage of infected cells at 24 hpi. Taken together, these observations indicate that full or partial deletion of *roaM*, or complementation with truncated *roaM*, induced more rapid cell-to-cell spread.

Truncation, deletion, and complementation with a truncated variant result in an increase in actin tail formation. Smaller plaque size of intracellular pathogens on host-cell monolayers has previously been correlated with loss of actin tails (14, 20). To determine if the differences in spread between strains are related to the production of actin tails, Vero cells were infected with *R. rickettsii* strains at an MOI of 0.5, fixed at 10 hpi, and stained with phalloidin to visualize actin tail production (Fig. 3A). Quantification of actin tail production was accomplished using Imaris cell imaging software to identify actin filaments associated with rickettsiae from z-stacks obtained on a wide-field microscope and then corrected for error by normalizing to the values for R_{cl} *sca2*::Tn (R_{cl} is R clear, a higher-passage derivative of R), which is known not to produce long actin tails (Fig. 3B) (20). SS_L, SS_S-Δ*roaM*, SS_S-pROAM-T, and R_{cl} produced actin tails at approximately three to four times the rate of SS_S. Conversely, SS_S-pROAM-FL produced almost no actin tails, although individual examples of SS_S-pROAM-FL generating actin tails could be found at later time points, such as 48 hpi (Fig. 3C). This suggests that the lower rate of actin tail formation in SS_S-pROAM-FL is not due to an overall inability to generate them.

Determination of *roaM* translation start site indicates that the large plaque size of the *R. rickettsii* Iowa strain is due to a previously identified point mutation. We investigated in detail the M4I nonsynonymous mutation in *roaM* in Iowa compared to Sheila Smith (26). The Iowa strain makes large, opaque plaques (27). The first four annotated amino acids in RoaM for Sheila Smith are MMSM, raising the possibility that more than one of these ATG codons could serve as the actual translation start site. To address this point, a reporter plasmid to measure promoter activity was constructed, pRrReporter (Fig. 4A). Promoter sequences up to the potential translational start site of interest were cloned into pRrReporter to drive the transcription and translation of GFPuv (green fluorescent protein with maximal fluorescence under UV light) (Fig. 4B). The guanidine residue highlighted in Fig. 4B was empirically determined by capping-RACE (rapid amplification of cDNA ends) (28) to be the transcriptional start site (Fig. S3). Measured fluorescence intensity can then be normalized to constitutively expressed mCherry, driven by the *rompA* promoter. Fluorescent microscopy images for the reporters in *Escherichia coli* and *R. rickettsii* (Fig. 4C) were quantified using FIJI image analysis (Fig. 4D and E). No variants of the *roaM* promoter were able to drive production of GFP in *E. coli* (Fig. 4D). In *R. rickettsii*, only P^{roaM} 3rd was able to produce detectable GFP fluorescence. This suggests that the third methionine is the actual first residue of RoaM. Subsequent numbering of amino acids here is based upon this translational start site.

Because P^{roaM} Iowa did not produce detectable GFP, the Iowa strain may not generate RoaM due to the nonsynonymous point mutation affecting the translational start site. To confirm this, a rabbit polyclonal antibody against RoaM was generated and used to probe Western blots of purified rickettsiae (Fig. 5A). Anti-RoaM detected a band in SS_S approximating the predicted size of 41.5 kDa, and a smaller band in SS_L close to the predicted size of truncated RoaM, 24.6 kDa. Preincubation of the antibody with the immunizing peptide antigen inhibited antibody binding to either the full-length or truncated RoaM, thus demonstrating specificity of the reaction. No bands were detected for SS_S-Δ*roaM* or Iowa, indicating that Iowa does not produce significant amounts of RoaM. The transcription of *roaM* was also tested by amplifying PCR fragments from cDNA internal to *roaM*, *A1G_06525*, and *gltA* as a control (Fig. 5B). SS_S-Δ*roaM* does not produce the fragment corresponding to *roaM* but does transcribe *A1G_06525*, likely as readthrough from the transcription of *gfp*uv. The Iowa strain produces transcripts for both *roaM* and *A1G_06525*, even though it does not translate *roaM* in any significant amount. Note that *roaM* and *A1G_06525* are predicted to be transcribed as an operon (29), and PCR amplification from rickettsial cDNA using a

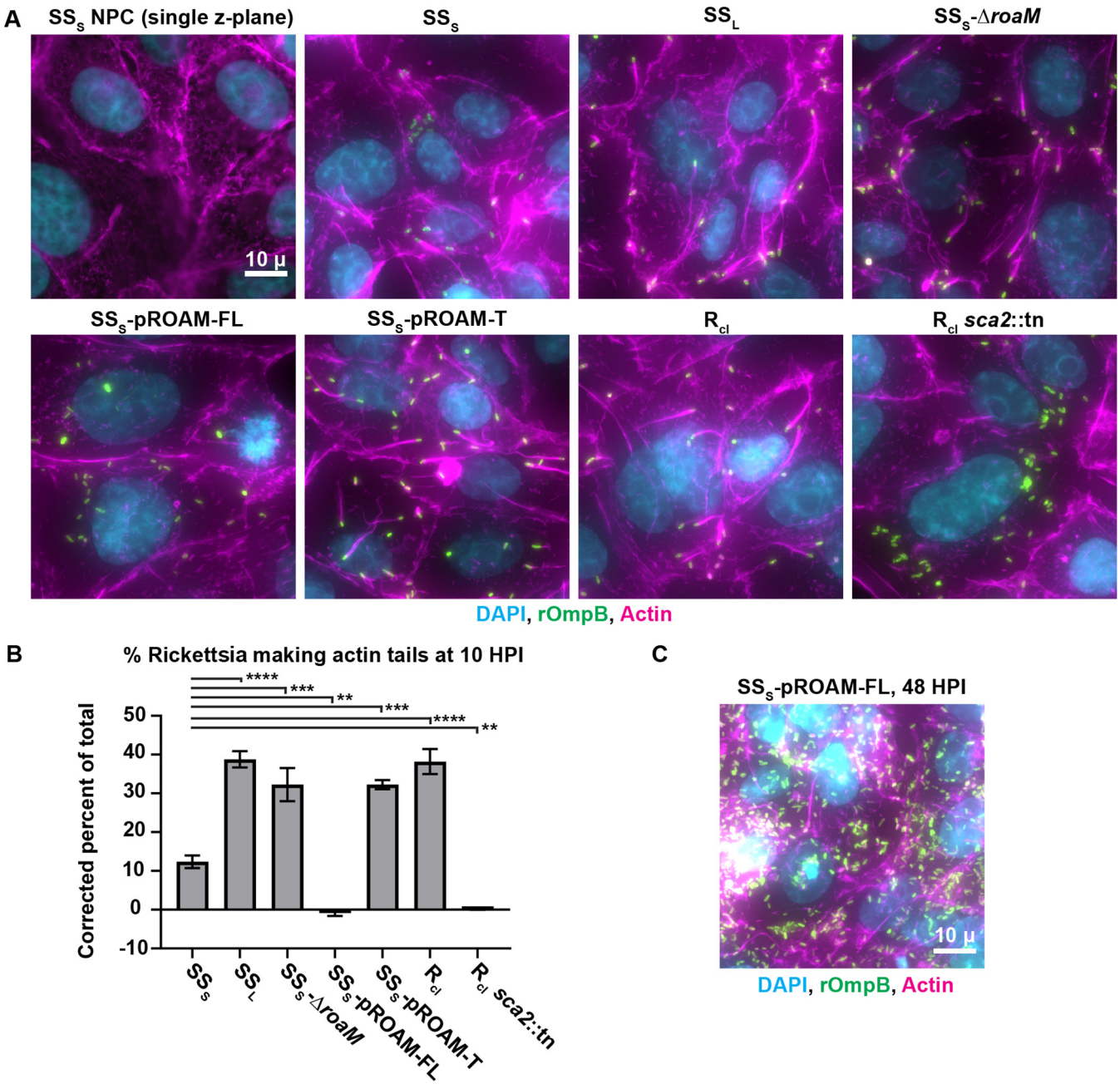

FIG 3 Ablation of *roaM* or complementation with a truncated variant results in an increased rate of actin-tail formation. Vero 76 cell monolayers on coverslips were infected with *R. rickettsii* at an MOI of 0.5 and fixed with paraformaldehyde at 10 or 48 h postinfection. IFAs were performed, visualizing actin with phalloidin-Alexa Fluor 568 (magenta) and rickettsiae with MAb13-2 (green) and using DAPI as a nuclear stain (cyan). (A) Representative maximum intensity projections derived from wide-field images showing production of actin tails by different *R. rickettsii* strains at 10 h postinfection. The control with no primary antibody to rickettsiae (NPC) is a single, representative z-plane. (B) Three independent experiments, each with five randomly acquired z-stacks for each strain, were analyzed using Imaris 9.7 to automatically identify rickettsiae and actin filaments likely to be tails (by filtering for size and sphericity). Each experiment was corrected for error by subtracting the results for production of tails by the *sca2* mutant, which is known to not generate any large actin tails (20). The resulting data matched results from a manually annotated subset. Error bars represent standard errors of the means. Standard ANOVA followed by Dunnett's multiple-comparison test was used to determine the significance of results compared to SS$_S$. ****, $P \leq 0.0001$; ***, $P = 0.0002$; **, $P = 0.005$ to 0.01. (C) Representative maximum intensity projection derived from a wide-field acquired z-stack showing actin tail production by SS$_S$-pROAM-FL at 48 h postinfection.

primer pair with annealing sites internal to *roaM* and internal to *A1G_06525* produce a band, confirming the transcript as polycistronic (Fig. S4).

RoaM is localized to the bacterial cytosol and is not secreted. To establish whether RoaM is secreted, we generated a SS$_S$ strain expressing glycogen synthase kinase 3β (GSK-3β)-tagged RoaM FL. This strategy was previously used (30) to determine

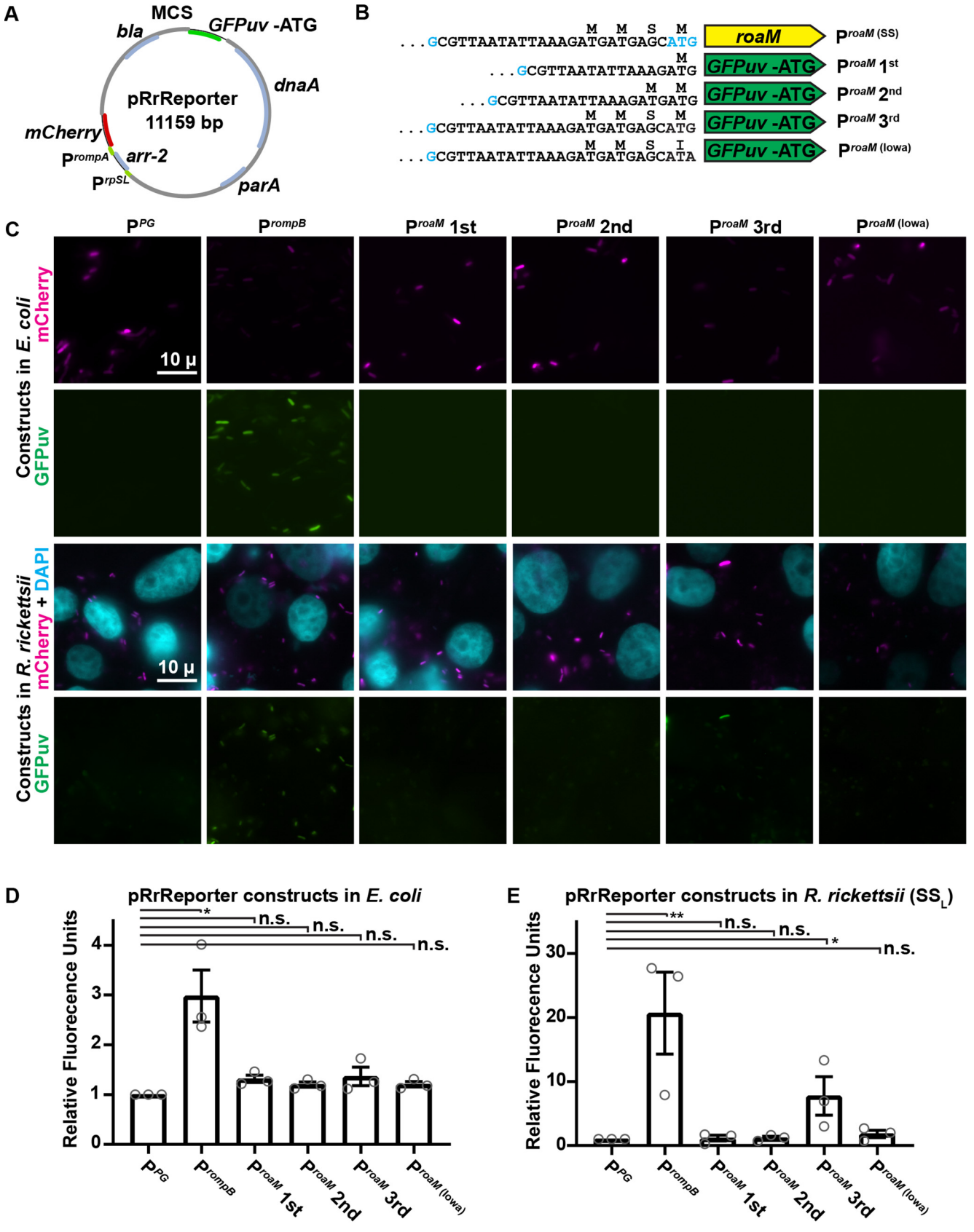

FIG 4 Determination of *roaM* translational start site via promoter-driven fluorescence analysis. (A) Schematic of the pRrReporter plasmid. (B) Diagram of the *roaM* promoter in SS_S and variant promoters cloned into pRrReporter to generate different reporter plasmids. (C) Representative wide-field microscopy

(Continued on next page)

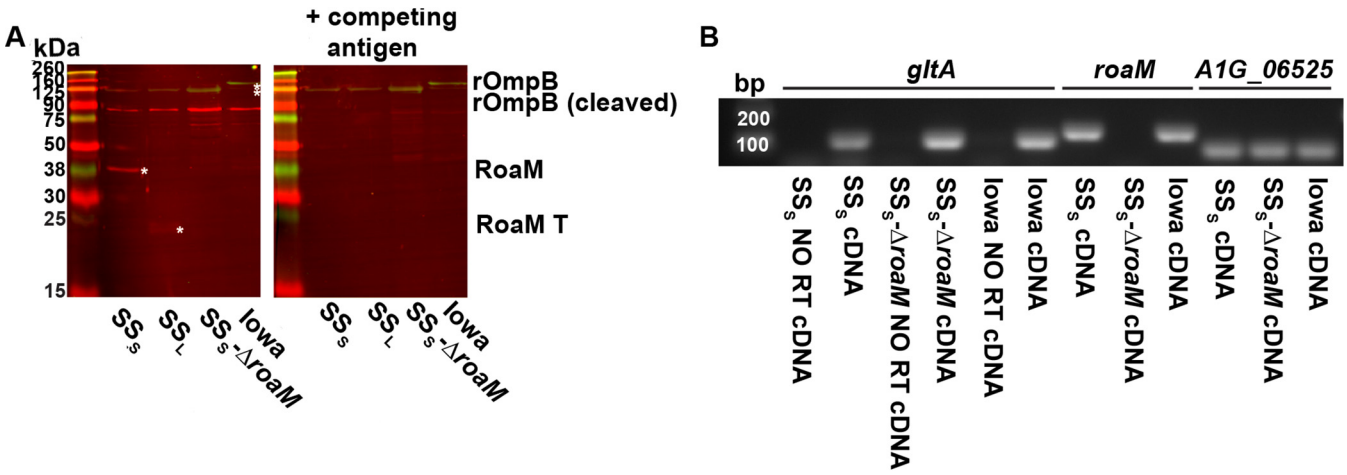

FIG 5 *R. rickettsii* Iowa does not produce RoaM despite transcribing *roaM*. (A) Western blot of samples solubilized in 2× Laemmli sample buffer and probed with anti-RoaM (red) and MAb 13-2 (green) with or without 5 μg/mL competing peptide antigen. White stars indicate full-length and truncated RoaM. (B) Agarose gel of PCR products for *gltA*, *roaM*, and *A1G_06525* from cDNA derived from SS_S, SS_S-Δ*roaM*, and Iowa strains.

that *R. rickettsii* RARP2 is a secreted effector. If a protein of interest is secreted and exposed to host cytosol, the GSK tag will be phosphorylated. A Western blot using total versus phospho-specific GSK-3β antibodies is used to determine the phosphorylation status of the protein. In the case of GSK-RoaM FL, we did not detect a phosphorylated band (Fig. 6A). By way of confirmation, we also utilized our FLAG-tagged RoaM strains in immunofluorescence assays (IFA). We found that the FLAG epitope from our nonsecreted control and RoaM variants could be detected within rickettsiae only when a lysozyme treatment and additional permeabilization step was added (Fig. 6B, compare upper to lower panels). The pattern of localization of RoaM appears to match that of FLAG-SS-MTase (30), a methyltransferase that is not secreted and is predicted to be localized to the rickettsial cytosol. Taken together, the results of these two experiments suggest that RoaM is not secreted.

Real-time quantitative PCR reveals no *roaM*-dependent reduction in expression level of genes implicated in actin-based motility or cell-to-cell spread. To determine whether RoaM reduces the formation of actin tails by inducing transcriptional repression of genes important for actin-based motility and spread, the expression of *sca2*, *rickA*, and *sca4* between strains was assessed by qRT-PCR (Fig. 7). Sca2 and RickA are involved in the polymerization of actin (20, 23, 31, 32), and thus, overexpression of either of these genes might have accounted for the increase in actin tail formation for some strains. Additionally, Sca4 mediates cell-to-cell spread by *R. parkeri* by interacting with vinculin to decrease the physical tension at cell-cell junctions and allow membrane protrusions into neighboring cells (33); therefore, its overexpression could also provide a partial explanation for the observed differences in actin-based motility between *roaM* mutants. Instead, no significant overexpression of *sca2*, *rickA*, or *sca4* was observed between strains when normalized to either of two control genes, *gltA* and *rpoD*. Likewise, for SS_S-pROAM-FL, no significant repression of these genes was observed. Based on these data, we conclude that it is unlikely that RoaM acts at the level of transcriptional regulation of these known actin-regulating genes. However, other unknown factors may be regulated by RoaM.

FIG 4 Legend (Continued)
images of reporter constructs in *E. coli* and *R. rickettsii*. Images were acquired with identical microscopy parameters, and brightness/contrast were adjusted uniformly for all images within bacterial species. (D and E) Quantification of GFP expression normalized to mCherry expression for reporter constructs in *E. coli* (D) and *R. rickettsii* (E) and the average relative intensity for identified bacteria was obtained for three independent experiments, each utilizing three fields per strain. The data were subsequently normalized to an unexpressed, putative pseudogene (PG). Brown-Forsythe and Welch ANOVA with Dunnett's multiple-comparison tests were performed on the prenormalized data. **, $P = 0.0044$; *, $P \leq 0.0214$; n.s. not significant. Error bars represent standard errors of the means.

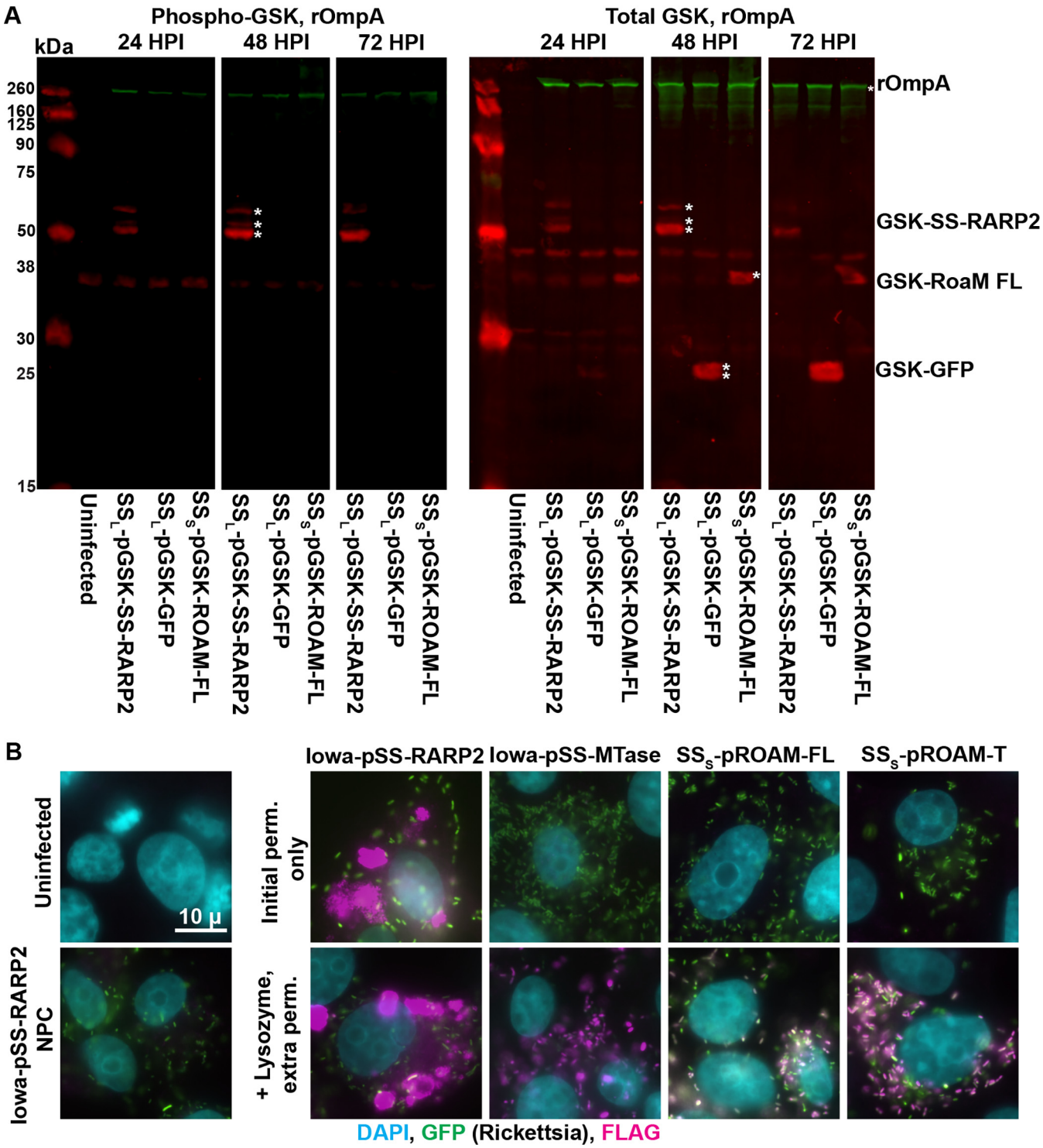

FIG 6 RoaM is not secreted by *R. rickettsii*. (A) Western blots of Vero 76 cell lysates infected with *R. rickettsii* expressing GSK-tagged proteins. Cells were infected at an MOI of 1, and lysates were prepared at 24, 48, and 72 hpi. Samples were run on duplicate gels and probed for phosphorylated (left) and total (right) GSK-tagged protein (red). MAb 13-3 against rOmpA (green) (66) was used as a loading control. Images are representative of three independent experiments. White stars in the 48-hpi panels indicate GSK-SS-RARP2, GSK-RoaM-FL, and GSK-GFP and proteolytic fragments of each. (B) Immunofluorescence assay for *R. rickettsii* Iowa expressing Sheila Smith RARP2 (Iowa-pSS-RARP2) (positive control for secretion), *R. rickettsii* Iowa expressing *Rrlowa_1431* (Iowa-pSS-MTase) (negative control for secretion) (30), and SS_S-pROAM-FL and SS_S-pROAM-T probed with anti-FLAG to visualize localization of ectopically expressed FLAG-tagged proteins. Cells shown in upper right images were permeabilized with 0.1% Triton x-100 only; those in lower right images were additionally treated with lysozyme and a secondary 0.1% Triton X-100 permeabilization. Uninfected and Iowa-pSS-RARP2 no-primary-antibody control samples underwent lysozyme treatment and secondary permeabilization steps. Large pleomorphic structures in Iowa-pSS-RARP2 panel are endoplasmic reticulum-derived structures resulting from expression of SS-RARP2 (30).

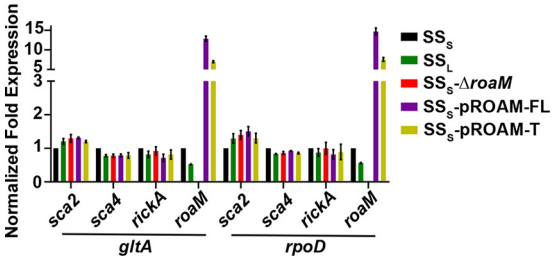

FIG 7 *roaM* expression has no discernible effect on the transcription of rickettsial genes known to influence motility or cell-to-cell spread. Three combined independent qRT-PCR experiments comparing the expression of *sca2*, *sca4*, and *rickA* normalized to *gltA* or *rpoD* for different *R. rickettsii* strains, with various *roaM* expression shown as an experimental control. Error bars represent standard deviations. Data were analyzed by two-way ANOVA followed by Dunnett's multiple-comparison test revealing no significance for the expression of *sca2*, *sca4*, and *rickA* for strains compared to SS$_S$ with the exception of one comparison; the difference in *sca2* expression between SS$_S$ and SS$_S$-pROAM-FL normalized to *rpoD*, with a *P* value of 0.0183. Each qRT-PCR experiment included three technical replicates per data point and controls without cDNA, negative controls without reverse transcriptase, and positive controls with gDNA to validate the results of the experiment. Melting curves were examined to ensure fidelity of each primer set.

Examples of both full-length and truncated *roaM* are found bioinformatically within different rickettsial species, and *roaM* genotype is predictive of plaque size phenotype in other *R. rickettsii* strains. Using genomic sequences available on the PATRIC bioinformatics resource center (34), we compared the state of the operon containing *roaM* and *A1G_06525* in different isolates of several *Rickettsia* spp. (Fig. 8). When genomic sequences of multiple isolates are available for the same species, it is often possible to find examples where the full-length *roaM* is present and others where it is ablated. This suggests that *roaM* may be mutated during different linages and passage histories. In the case of *R. heilongjiangensis*, the type strain 054, which has been maintained in Vero cells since its isolation in 1982, was sequenced in 2011 (35) and contains a truncated version of *roaM*. By comparison, *R. heilongjiangensis* isolated directly from multiple individual ticks and genomically sequenced contained full-length *roaM* homologs (36). These observations suggest that *roaM* may be selected against during repeated passage in cell culture.

To determine if the integrity of *roaM* could broadly predict plaque size for other isolates of *R. rickettsii*, we plaqued other strains in our collection on Vero cell monolayers (Fig. 9A) and measured the area of 50 plaques for each strain (Fig. 9B). The *roaM/A1G_06525* operon was PCR amplified from isolated genomic DNA and Sanger sequenced (Fig. 9C). An association was observed between truncations of *roaM* and a larger plaque size among *R. rickettsii* isolates.

Serial passage of *R. rickettsii* Sheila Smith small in Vero cells results in the spontaneous generation of *roaM* mutants. To determine if we could recapitulate the loss of *roaM* in cell culture, SS$_S$ was serially passaged every 3 to 4 days in Vero cells over a 5-week period. Three separate lineages were maintained. Large, clear plaques were first detected by passage 6. These plaque variants were readily apparent by the eighth passage and became more abundant over subsequent passages (Fig. 10A and B). For each lineage, a large clear plaque was isolated from passage 10 and subcloned twice. Sanger sequencing of the *roaM* region from DNA amplified from each of these plaques revealed that each lineage developed a novel mutation in *roaM* (Fig. 10C). The ease with which we were able to generate phenotypically large, clear plaques and associated mutations in *roaM* suggests that there is strong negative selection of *roaM* when *R. rickettsii* is cultured in Vero cells.

Overexpression of full-length RoaM delays onset and duration of fever in guinea pigs. To determine the impact of various *roaM* genotypes on virulence, groups of three female Hartley guinea pigs were each inoculated intradermally with 100 PFU of the given strains, and temperature was monitored daily via a subdermal transponder (Fig. 11). Guinea pigs infected with most strains developed an appreciable increase in fever between days 3 and 4, except for those with SS$_S$-pROAM-FL, for which the increase in fever began between days 6 and 7. The duration of fever for SS$_S$-pROAM-FL was 6 days compared to 7 to 9 days for the other strains. The delayed onset and

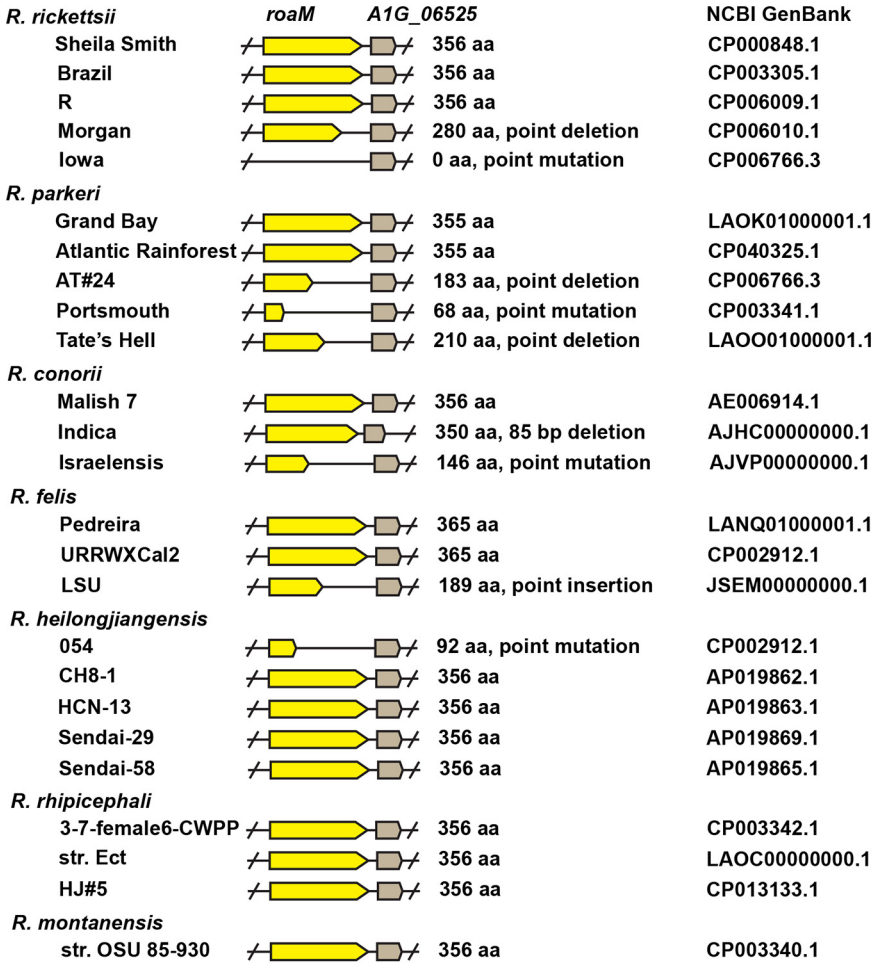

FIG 8 Annotated genotype of *roaM* in various *Rickettsia* spp. and isolates. Schematic of *roaM* and *A1G_06525* operons from various *Rickettsia* spp. and isolates based on annotated genomes on PATRIC (34). Yellow bars indicate the approximate length of the truncated *roaM* mutants. Critical mutations, differences between isolates, and the translated size of RoaM are listed to the right.

shorter duration of fever for guinea pigs infected with SS_S-pROAM-FL suggests that the observed reduction in actin tail formation for this strain *in vitro* may account for a decrease in overall virulence.

DISCUSSION

Here, we describe RoaM, a previously unknown regulator of actin dynamics in *Rickettsia* spp. RoaM was first identified in genomic comparisons as one of the few genes differing between the avirulent Iowa strain and virulent Sheila Smith, Morgan, and R strains of *R. rickettsii* (25, 26). Subsequent bioinformatic analysis of *roaM* from different spotted fever group rickettsiae revealed a mix of full-length and truncated versions of the gene, often from within the same rickettsial species. Where passage history was available, it appeared that minimally passaged strains were more likely to possess a full-length copy. Genetic disruption of *roaM* or expression of full-length and truncated versions indicated that RoaM is implicated in plaque size and actin-based motility. RoaM was not secreted from the rickettsiae and thus does not appear to directly interact with actin. Transcriptional analysis showed no effect of RoaM on expression levels of known rickettsial actin-interacting genes, thus suggesting that additional, unknown, regulatory mechanisms control actin-based motility in rickettsiae.

The disruption of *roaM* in *R. rickettsii* Sheila Smith resulted in larger plaque sizes and increased frequency of actin tail formation but no increase in virulence in a guinea

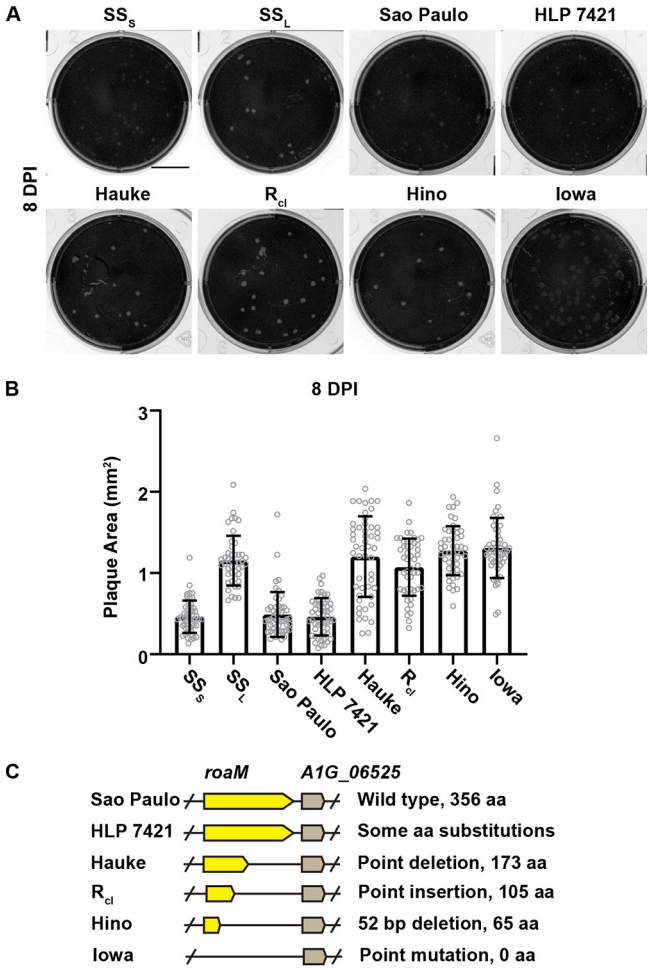

FIG 9 Genotype of *roaM* in *R. rickettsii* strains is correlative with plaque size. (A) Photographs of *R. rickettsii* plaques from different strains. Bar = 1 cm. (B) Measured plaque area for *R. rickettsii* strains at 8 days postinfection. Results represent a single experiment where 50 plaques were measured for each strain. Error bars represent standard deviations. One-way ANOVA (Kruskal-Wallis) followed by Dunn's multiple-comparison test was performed. The average plaque area for SS_S was significantly different ($<$0.0001) from that for SS_L, Hauke, Hino, Rcl, and Iowa, while plaque areas for Sao Paulo and HLP 7421 were not significantly different. Hauke, Hino, R_{cl}, and Iowa were not significantly different from SS_L. (C) Schematic of the *roaM*- and *A1G_06525*-containing operon as empirically determined by PCR amplification and Sanger sequencing. Mutations and overall amino acid length of RoaM are listed on the right.

pig model of infection. However, overexpression of *roaM* resulted in even smaller plaques than in the wild-type SS_S and decreased frequency of actin tail formation. In the case of *roaM* overexpression, we observed a modest reduction in fever response and duration of symptoms. Although plaque size can be a useful phenotype and may be indicative of changes in actin-based motility, it does not necessarily equate with virulence. For example, in the Iowa strain, small- and large-plaque variants have been isolated, yet neither is virulent in guinea pigs (24), presumably due to the multiple mutations observed in comparison to virulent strains (26). Similarly, both clear (lytic) and opaque (nonlytic) plaque phenotypes have been isolated from both the virulent R strain and avirulent Iowa strains of *R. rickettsii*, yet neither plaque phenotype differs in virulence from the parental strain (21).

As obligately intracellular pathogens, *Rickettsia* spp. possess a relatively minimized genome and have been hypothesized to be in a perpetual state of genome reduction due largely to their dependence upon the host for many nutrients and growth factors that they would otherwise need to synthesize (37). In the case of agents of vector-borne diseases, complex interactions with the host and vector likely impose positive or

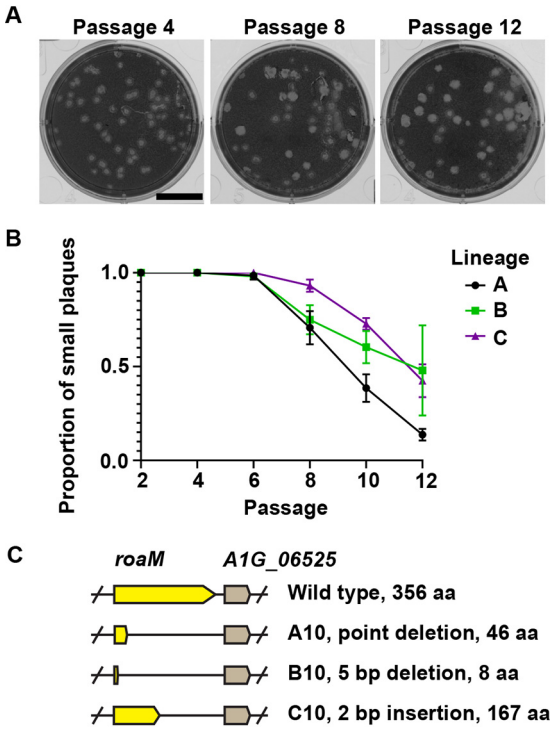

FIG 10 Serial passage of SS_S in Vero cells leads to *roaM* mutations and an emergent large-plaque phenotype. Three separate linages were maintained. (A) Examples of plaques at passages 4, 8, and 12 from lineage B. Bar = 1 cm. (B) Ratios of small to large, clear plaques for lineages A, B, and C over successive passages. Each data point represents the average of two replicate wells, and error bars represent standard deviations. (C) Schematic of operon containing *roaM* and *A1G_06525*, which were PCR amplified from a single large, clear isolated plaque from passage 10 of each lineage and subsequently Sanger sequenced. Mutations and overall amino acid length of RoaM are listed on the right.

negative selective pressure on different genes (38). Extended laboratory passage of facultative intracellular bacterial pathogens (39–43) is well known to frequently lead to a loss of virulence factors due to the absence of host-imposed selective pressures. A more complex dynamic may exist in vector-borne diseases. The interesting possibility arises that certain rickettsial genes may be essential in either the vector or the host but detrimental in the other and, thus, a balance must be achieved. Wild-type *roaM* seems to be found in fresh isolates of *R. rickettsii* but appears to be strongly selected against during cell culture passage. The rapid loss of *roaM* during laboratory passage was recapitulated experimentally in Vero cells. This suggests that there are rickettsial genes

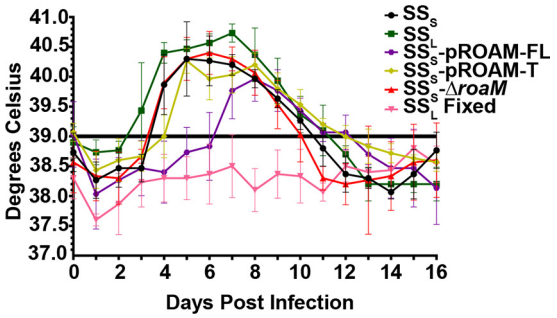

FIG 11 Overexpression of RoaM delays onset and duration of fever in guinea pigs. Three guinea pigs per strain were challenged intradermally with 100 PFU of *R. rickettsii*. Temperature was monitored by intradermal transponder. Values are means and standard deviations. Guinea pigs became febrile between days 3 and 4 for most strains and exhibited subsidence of fever by day 11. Animals infected with the overexpressing SS_S-pROAM-FL strain showed a delayed onset and shorter duration of fever.

essential in the tick reservoir that are unnecessary or even deleterious in mammalian hosts. The strong negative selective pressure against RoaM in Vero cells may explain our failure to complement the SS_5-Δ*roaM* mutant with full-length *roaM* despite repeated efforts.

Other rickettsial genes, such as that encoding a major surface antigen, rOmpA, appear to have been lost from the Iowa strain of *R. rickettsii* (24–26). The Iowa strain is unique in that it has been passed 271 times through embryonated chicken eggs. It was originally described as mildly virulent and then as having increased virulence and then became avirulent (44). The original isolate is no longer available, and most of these studies were done before plaque purification of rickettsiae was developed. Later, a targeted knockout of *rompA* revealed that *rompA* is not essential for virulence in a guinea pig model. It was speculated that the gene might be necessary for maintenance in of *R. rickettsii* in ticks (45); however, the recognition that *rompA* is disrupted in *Rickettsia peacockii* (46, 47), a commensal in ticks, suggests that may not be the case.

It is also possible that there are rickettsial genes necessary for survival or virulence in mammalian cells that are superfluous in ticks. Certainly, virulent strains of *R. rickettsii* can be detrimental to the tick vector. The death of *Dermacentor andersoni* infected with *R. rickettsii* was noted by Burgdorfer in 1963 (48), and a more thorough study by Niebylski et al. (49) showed a very high mortality rate for infected ticks and introduced the effects of temperature on the survival of infected ticks. Labruna et al. similarly found that infection of *Amblyomma aureolatum* with the sympatric strain *R. rickettsii* Taiaçu also resulted in mortality and reduced oviposition of infected ticks (50). Still other studies using different tick-*Rickettsia* sp. combinations have found minimal or no apparent effects of rickettsial infection on the arthropod vector (51–54). Although many of the differences in these studies may be accounted for by the differences between tick species, infection with a rickettsia lacking a mechanism to check its activation of actin-based motility could be responsible for additional cellular damage to the vector, leading to decreased survival. Although not confirmed experimentally, it is conceivable that extended passage through ticks could select against rickettsial genes essential in mammals but not required in ticks. Such a mechanism could explain the existence of rickettsial species such as *R. peacockii*, which is transmitted transovarially in ticks yet for which there is no evidence for transmission to mammals and which has not been propagated in mammalian cell culture (55, 56). Multiple genes thought to contribute to the virulence of *R. rickettsii*, including *rarP2*, *rompA*, *sca1*, *rickA*, *dsbA*, the protease II gene, and a putative phosphoethanolamine transferase gene (47), are deleted in *R. peacockii*.

The effects on virulence of *R. rickettsii* after serial passage in different hosts or vectors may have been presaged by Price in the 1950s (57). Virulent strains passaged by spleen transfer through cottontail rabbits, a target of *Haemaphysalis leporispalustris* ticks resulted in decreased virulence. These data were recapitulated for both dogs and opossums (57). However, these strains were able to maintain their virulence if passed through cottontail rabbits from one animal to another via *Dermacentor andersoni* nymphs. Perhaps this series of experiments was an early indicator that there are important selective pressures inherent in the environment within the tick. It is possible that the difference in selective pressures might be leveraged as a tool to explore loss or gain of function under various culture conditions (58). Serial passage in different arthropod and mammalian cell types or whole animals may reveal mutations in genes important for managing the relationship between bacterium, host, and vector. There have been several alternative methods for the culture of *Rickettsia* spp. explored using tick and mosquito cell lines (56, 59), and these methods might provide greater genomic stability or a different menu of selective pressures for gene loss than mammalian cell culture.

The observation that disruption of RoaM can increase actin tail formation and cell-to-cell motility has implications for the interpretation of studies in actin-based motility that rely on measurement and characterization of actin tails. An allele strongly

downregulating tails in some situations could also exist, and because the stimulus for turning actin motility on or off is not yet known, this could result in the appearance of being immotile, as *R. peacockii* appears to be despite possessing *sca2*. Clearly, *roaM* presents a confounding factor that will need to be resolved for future actin-based motility studies in *Rickettsia* species. An additional consequence is that *R. rickettsii roaM* mutants produce large, robust plaques, which may lead to unintentional selection during plaque isolation procedures. The unknowing usage of hyperspreading mutants may also have consequences for the survival and fecundity of the arthropod vector.

If rickettsiae containing wild-type *roaM* are able to regulate their cell-to-cell spread, it would not be surprising to find that the reason for this is to more efficiently utilize the resources in a particular host cell until those resources become limiting. At such a time, an unknown signal may cause *Rickettsia* to activate its motility. RoaM is cytosolic, and it has no effect on the transcription of known rickettsial genes related to motility, although a broader screen will be necessary to rule out a possible role as a transcriptional regulator. The functional mechanism of RoaM may otherwise be based on protein-protein interactions or signaling. Some clues may be inferred from ectopic expression of RoaM T resulting in increased motility. RoaM T could achieve this phenotypic effect by multimerizing incorrectly with wild-type RoaM. Alternatively, if RoaM and A1G_06525 interact, as might be inferred from their synteny, overexpression of RoaM T may titrate A1G_065525 away from its normal function, where it would interact with wild-type RoaM. Recent work with *Rickettsia parkeri* has shown that actin tails disengage when in a protrusion before entry into an adjacent cell (33), and here may be an instance where RoaM might negatively regulate actin tails. Both Phyre2 and DELTA-BLAST suggest a small degree of structural similarity to the myosin heavy chain (60, 61). It is tempting to speculate whether RoaM might have a similar structural role and perhaps be involved in mechanosensing, similar to myosins (62). Future work will necessarily be driven by the need to reveal the mechanism by which RoaM regulates actin-based motility and is likely to identify additional factors controlling actin-based motility.

MATERIALS AND METHODS

Cell lines and rickettsiae. Vero76 cells (ATCC CCL-81) were grown in RPMI medium plus 5% heat-inactivated fetal bovine serum (FBS) at 37°C in a 5% CO_2 atmosphere. *Rickettsia rickettsii* Sheila Smith (CP000848.1) organisms were grown at 34°C in Vero 76 cells in M199 medium plus 2% heat-inactivated FBS in a 5% CO_2 atmosphere. For purification of rickettsiae, infected Vero cells were lysed by Dounce homogenization followed by centrifugation through a 30% Renografin pad. Rickettsiae were washed twice in 250 mM sucrose and stored in brain heart infusion broth (BHI) at −80°C. Each rickettsial stock was titrated for PFU by plaque assay. For plaque assays, Vero cells were grown to monolayers in 6-well plates in RPMI 1640 medium with 5% FBS as previously described (19, 20). The medium was removed, and 100 μl of *R. rickettsii*-containing BHI dilutions was added directly to each well. Plates were incubated for 30 min at 34°C and 5% CO_2. Vero cells and *R. rickettsii* dilutions were overlaid with 5 mL of M199 medium with 5% FBS and molten 0.5% low-melting-point agarose and were grown for 5 days at 34°C and 5% CO_2. Wells with visible plaques were stained with 0.5 mL thiazolyl blue tetrazolium bromide (MTT; 0.3 mg/mL in K36 buffer) overnight, PFU were counted the next day, and PFU/mL were calculated. PFU were used to calculate multiplicities of infection (MOI).

Strain histories of *R. rickettsii* from the RML culture collection used here are listed in Table 1.

PCR amplification and plasmid and genomic DNA isolation. PCR products were amplified from target DNA using primers ordered from Integrated DNA Technologies (Table S3) with Q5 high-fidelity DNA polymerase (New England Biolabs [NEB], M0491), isolated using a GeneJet PCR purification kit (Thermo Scientific, K0702), and ligated into vector backbones using T4 DNA ligase (NEB, M0202), all per manufacturers' instructions. Generated plasmids were transformed into NEB stable competent *E. coli* (NEB, C3040H) and were prepared using GeneJet plasmid miniprep or maxiprep kits (Thermo Scientific, K0503 and K0492). Isolation of rickettsial genomic DNA was accomplished by processing individual stock aliquots with the DNeasy blood and tissue kit (Qiagen, 69504). Sanger sequencing to confirm constructs and PCR products derived from genomic DNA were performed by ACGT Inc.

Construction of *R. rickettsii* strains. Plasmids pROAM-FL and pROAM-T were generated from pRAMF2-N and transformed into the small-clone variant of Sheila Smith (SS_5) to constitutively overexpress full-length and truncated RoaM (Fig. S1). A genetic knockout of *roaM* was generated via recombination with a plasmid-based cassette expressing GFP and rifampin resistance. The strategy employed was based on the FRAEM method employed for *Chlamydia* (63). Briefly, a cassette consisting of constitutively expressed GFP and rifampin resistance genes flanked by two regions of homology (2,039 bp upstream and 1,433 bp downstream) flanking the knockout target, *roaM*, were cloned into pRKO

TABLE 1 Strain histories of *R. rickettsii* in the Rocky Mountain Laboratories collection used here

Strain	Passage history[a]	Clone	*roaM*[b]
Sheila Smith (SS) (1961 seed)	5EP/4VC	1	FL
SS_S	5EP/4VC/1MP/11VC	1	FL
SS_L	5EP/4VC/1MP/14VC	2	T
R_{cl}[c]	10EP/3VC/1 MP /12VC	1	T
R_{cl} #9-7 Sca2 KO	10EP/3VC/1 MP /17VC	#9-7	T
Iowa	271EP/1GP/9VC/1MP/14VC	1	T
Sao Paulo	8EP/4VC/1MP/6VC	1	FL
HLP 7421	7EP/6VC/1MP/5VC	2	FL
Hauke	?/1TC/7VC	1	T
Hino	?/5EP/8VC	1	T

[a]Number of passages in embryonated eggs (EP), Vero cells (VC), BALB/c mice (MP), guinea pig (GP), and tissue culture (TC). ?, unknown number of passages.
[b]Genotype of *roaM*. FL, full length; T, truncated (truncation varies with strain; see the text).
[c]R clear (R_{cl}) is a higher-passage derivative of R. It is the strain transposon mutagenized to generate the Sca2 knockout (20).

(Fig. S2A). This fragment was then cloned into a backbone that constitutively expresses mCherry. After transformation and passaging, homologous recombination was selected for by picking GFP-positive, mCherry-negative plaques. This strategy was, however, unsuccessful in generating knockouts of other genes, including a putative pseudogene and genes where knockouts have already been generated via transposon mutagenesis.

Growth curves for *R. rickettsii* strains. For each strain, five 25-cm^2 flasks of confluent Vero cells were infected at an MOI of 0.25 and rocked at room temperature for 30 min. Eight milliliters of M199 with 2% FBS was then added, and flasks were incubated at 34°C. To harvest, medium was removed, and cells were scraped into 1 mL of BHI. Specimens were added to a microcentrifuge tube containing presterilized glass beads, and host cells were disrupted by using a Mini Beadbeater (BioSpec Products) for 10 s. Samples were divided and stored at −80°C in an isopropanol cooler until quantitation of PFU.

Plaque size measurements. To determine average plaque size for various *R. rickettsii* strains, Vero cells in six-well plates were infected with rickettsiae diluted in BHI such that approximately 10 to 40 plaques per well were obtained. Plates were stained with MTT (0.3 mg/mL in K36 buffer) at 8 or 15 days postinfection. Plaques were imaged on a Bio-Rad ChemiDoc MP system with transillumination. The diameter of plaques was measured with a digital caliper (Mitutoyo, 500-171-30) at a consistent horizontal angle, from top to bottom, left to right, to avoid bias.

SDS-PAGE and Western blotting. Rickettsia-infected Vero 76 cell lysates were generated by adding 100 μL 2× Laemmli buffer (64) per well of a 24-well plate. Samples were inactivated by heating at 99°C for 10 min. Samples were run on an SDS-PAGE gel and transferred to a polyvinylidene difluoride (PVDF) membrane at 100 V for 1 h and 15 min in Towbin transfer buffer (65) containing 20% methanol. Membranes were dried overnight, briefly rehydrated in methanol, rinsed with Tris-buffered saline (TBS), and blocked for 1 h in Odyssey blocking buffer (Li-Cor, 927-50000) at room temperature. Primary antibodies were diluted in blocking buffer with 0.2% Tween 20, while secondary antibodies IRDye 680RD goat anti-rabbit immunoglobulin and IRDye 800CW goat anti-mouse immunoglobulin (Li-Cor, 926-68071 and 926-32210) were diluted 1:10,000 in blocking buffer with 0.2% Tween 20 and 0.02% SDS. Blots were then visualized on an Odyssey CLx system and analyzed in Image Studio 5.2 (Li-Cor).

Secretion of RoaM was assayed utilizing GSK-tagged proteins as described previously (30). Vero 76 cells were grown in a 24-well plate and infected with GSK-tagged protein expressing strains of *R. rickettsii* at an MOI of 1 for 24, 48, and 72 h before harvesting in Laemmli sample buffer as described above. Western blots were probed with anti-phospho-GSK-3β (1:1,000) (Cell Signaling Technology, 5558) to detect phosphorylation of the GSK tag or anti-GSK-3β tag (1:1,000) (Cell Signaling Technology, 9325) as a control for production of the GSK-tagged proteins. Monoclonal antibody (MAb) 13-3 (1:1,000) was used as a loading control for rickettsiae.

Generation of RoaM polyclonal antibodies. Polyclonal antibodies to RoaM were generated commercially (GenScript) by immunizing two New Zealand White rabbits with a three-booster series of 0.2 mg keyhole limpet hemocyanin (KLH)-conjugated synthetic peptide derived from RoaM (NREILTHEEIFKC) predicted to be antigenic by a proprietary algorithm (GenScript). A C-terminal cysteine was added to aid in conjugation to the KLH. Sera were collected and antigen affinity purified.

Immunofluorescence assays and microscopy. Vero cell monolayers were grown on round 12-mm no. 1.5 coverslips (Glaswarenfabrik Karl Hecht GmbH & Co. KG) in 24-well plates using RPMI medium with 5% FBS. Monolayers were infected at the desired MOI as specified in the figure legends and synchronized by centrifuging at 750 × *g* at room temperature for 5 min followed by incubation at 34°C until the desired time point for analysis. Cultures were rinsed with 500 μL Hanks' balanced salt solution with Ca^{2+} and Mg^{2+} (Gibco, 14025076) and then fixed with either 1 mL 4% paraformaldehyde in PBS or 1 mL of methanol for 20 min. After permeabilization, blocking, and probing with specific antibodies, coverslips were mounted on slides using ProLong Diamond antifade mounting medium (Thermo Fisher, P36961). All immunofluorescence experiments incorporated controls to which no primary antibody was

added in order to control for potential nonspecific binding. Imaging was performed on a Nikon Ti2 Eclipse wide-field microscope equipped with a Nikon DS-Qi2 camera, Lumencor SOLA light engine, and Semrock filters DAPI-3060A, GFP-4050B, and LED-TRITC-A, using a Plan Apo λ 60× oil immersion objective with a numerical aperture (NA) of 1.4. Acquisition of random fields was accomplished using Nikon NIS-Elements Advanced Research version 5.11.02, autofocusing on the DAPI (4′,6-diamidino-2-phenylindole) channel.

A modified permeabilization strategy with FLAG-tagged constructs was also performed to assess localization of RoaM (30). Vero 76 cells were grown on coverslips in a 24-well plate and infected at an MOI of 1 with FLAG-tagged protein expressing *R. rickettsii* strains. After fixation at 48 h postinfection with 4% paraformaldehyde in PBS, all samples were permeabilized for 10 min with 250 μL Triton X-100 in PBS at room temperature. A subset of samples were then incubated with 1 mg/mL lysozyme in PBS (Sigma, L6876) for 10 min at room temperature, followed by an additional 10 min treatment with Triton X-100 in PBS at room temperature. Coverslips were probed with anti-FLAG (Sigma, F1804) (1:500 in PBS) for 1 h at room temperature, followed by 3 washes with 500 μL PBS and then goat anti-mouse IgG H&L (heavy plus light chain) conjugated to Alexa Fluor 568 (Abcam, ab175701) (1:500) for 1 h at room temperature. DAPI (1 μg/mL in PBS) was applied to each well for 5 min at room temperature as a counterstain. Each well was washed 3 times with 500 μL/well PBS before mounting in ProLong Diamond.

Analysis of *R. rickettsii* foci of infection. Vero 76 monolayers on glass coverslips in 24-well plates were infected at an MOI of 0.1. Cultures were rinsed with 500 μl of HBSS and then fixed and permeabilized with 1 mL/well methanol for 20 min at room temperature at 24 and 48 hpi. Specimens were then blocked with 250 μl 1% bovine serum albumin (BSA) for 1 h at room temperature, probed with 1 μg/mL MAb 13-2 (rOmpB) (66) and anti-Na/K ATPase (Abcam, ab76020; 1:500) in PBS, and incubated at 4°C overnight. Coverslips were washed 3 times with 500 μl of PBS, labeled with goat anti-mouse IgG H&L-Alexa Fluor 488 (1:500 in PBS) (Abcam, ab150117) and goat anti-rabbit IgG H&L-Alexa Fluor 568 (1:500 in PBS) (Abcam, ab175695) for 1 h at room temperature, and then counterstained with DAPI (1 μg/mL) for 5 min at room temperature. Coverslips were washed 3 times with 500 μL PBS before mounting in ProLong Diamond. Five random wide-field images were acquired for each strain and processed in Imaris 9.7.2. Individual cells were segmented based on the Na/K ATPase staining of the cell membrane and DAPI staining of the nucleus using the Imaris cell module to generate regions of interest. Rickettsiae were automatically identified and attributed to their respective regions of interest (ROI) to assess the number of rickettsiae and the percentage of infected cells per strain.

Quantification of actin tails. Vero 76 monolayers on glass coverslips were infected at an MOI of 0.5, incubated at 34°C in Vero 76 cells in M199 medium plus 2% heat-inactivated FBS in a 5% CO_2 atmosphere. Cultures were fixed at 10 hpi in 4% paraformaldehyde for 20 min at room temperature, permeabilized with 0.1% Triton X-100 for 15 min at room temperature, and then blocked with 1% BSA in PBS for 1 h. Coverslips were probed with 1 μg/mL MAb 13-2 in PBS overnight at room temperature. Coverslips were then washed 3 times with PBS and probed with goat anti-mouse IgG H&L-Alexa Fluor 488 1:400 in PBS (Abcam, ab150117) and Alexa Fluor 568 phalloidin (1:400 in PBS) (Thermo Fisher, A12380) for 3 h at room temperature. Coverslips were counterstained with 1 μg/mL DAPI for 5 min at room temperature. Coverslips were washed 3 times with 500 μL PBS before mounting in ProLong Diamond. Five random, wide-field 10-μm z-stacks were acquired in 0.27-μm steps for each strain. Actin tails were quantified using Imaris 9.7.2 by identifying phalloidin-stained actin filtered by mass and sphericity and then identifying rickettsiae that were located within 1.06 μm of the identified filaments. The 1.06-μm threshold for association between software-defined rickettsiae and actin filaments to define rickettsiae as producing tails was empirically determined by comparison to manually scored data subsets. Data were corrected for misidentification of actin filaments as tails in close proximity to *Rickettsia* by using *R. rickettsii* R_{cl} *sca2*::Tn, which does not produce actin tails (20). Manual scoring of three z-stacks for each strain from one experiment gave data equivalent to those obtained with the automated methodology.

***roaM* promoter analysis.** *R. rickettsii* strains carrying GFP reporter constructs were used to infect Vero 76 monolayers on coverslips at an MOI of 0.25 and fixed with 4% paraformaldehyde at 24 hpi. Rickettsia-infected cells were then permeabilized with 0.1% Triton X-100 for 5 min and counterstained with 1 μg/mL DAPI for 5 min. Coverslips were then washed 3 times with PBS before mounting in ProLong Diamond. before mounting. Overnight cultures of *E. coli* strains carrying reporter constructs were diluted 1:100 in LB and incubated for 3 h at 37°C. Samples were then diluted 1:50 in LB, and 5 μL of each sample was allowed to dry onto a coverslip before mounting in ProLong Diamond antifade mounting medium. For each experiment, three images were taken for each strain and processed with the FIJI distribution of ImageJ2 (67). ROI were generated by defining a mask based on the TRITC (tetramethyl rhodamine isocyanate) channel by applying a Gaussian blur with a sigma of 2, rolling ball background subtraction set to 50 pixels (rickettsiae only), and thresholding using the Otsu algorithm (68). The resulting ROI were then applied to the original GFP and TRITC channels to obtain intensity values for each individual ROI with an area between 0.5 and 10 pixels.

Generation of RoaM polyclonal antibodies. Polyclonal antibodies to RoaM were generated commercially (GenScript) by immunizing two New Zealand White rabbits with a three-booster series of 0.2 mg of a KLH-conjugated synthetic peptide derived from RoaM (NREILTHEEIFKC) predicted to be antigenic by a proprietary algorithm (GenScript). A C-terminal cysteine was added to aid in conjugation to the KLH. Sera were collected and antigen affinity purified.

***R. rickettsii* RNA isolation and RT-qPCR.** Vero cells were infected with *R. rickettsii* at an MOI of 0.1 and incubated for 48 h at 34°C. Medium was poured off, and cells were scraped into 1 mL PBS and centrifuged for 5 min at 3,000 × *g* in a microcentrifuge tube. The supernatant was removed, and the cell pellet was dissolved in 1 mL TRIzol LS reagent (Invitrogen, 10296028) preheated to 99°C. RNA was

extracted by using Direct-zol RNA Miniprep Plus (Zymo Research, R2070) following the manufacturer's protocols, including the on-column DNase I treatment. Each RNA sample was treated with 2 U of RNase-free DNase I (New England Biolabs, M0303) for 15 min at 37°C and then further purified using the RNA Clean & Concentrator-5 kit (Zymo Research, R1013) as per the manufacturer's protocol, including the on-column DNase I treatment. Purified RNA was assessed for quality with a NanoDrop 2000 spectrophotometer (Thermo Fisher). cDNA was generated using the SuperScript IV first-strand synthesis system (Invitrogen, 18091050) with 200 ng of RNA per sample, amplified with random hexamers, and RNase H was added as per the manufacturer's protocol. Controls run in the absence of reverse transcriptase were generated simultaneously. For qPCR, 20-μL reaction mixtures were assembled using SYBR green PCR master mix (Applied Biosystems, 4309155) with a 25 nM concentration of each primer (Table S3) and 2 μL cDNA. The program used was as follows: 10 min incubation at 95°C, followed by 40 cycles of 95°C for 15 s, 56°C for 30 s, and 60°C for 30 s. Amplification and melting curves for qPCR were performed on a Roche LightCycler 480, and cycle threshold (C_T) values were calculated with the LightCycler 480 software using the Absolute Quantification 2nd Derivative Maximum function. Genomic DNA (gDNA) positive controls and negative controls, including reactions in the absence of reverse transcriptase, and controls without cDNA were performed, and appropriate criteria for controls were met. C_T values were used to calculate $\Delta\Delta C_T$ fold effect relative to the control genes *gltA* and *rpoD* (69).

Determination of transcriptional start sites. To determine the transcriptional start sites of *roaM* and *sca5*/*ompB*, the capping-RACE method was utilized (28, 70). Briefly, RNA was isolated from infected cells as above, and a 5′ cap structure was added to approximately 5 μg of RNA using vaccinia capping enzyme (NEB, M2080S) per the manufacturer's instructions. RNA was reisolated from this reaction mixture using an RNA Clean and Concentrator-5 kit (Zymo Research, R1013). Approximately 100 ng of capped RNA was incubated with 2 pmol gene-specific primer for either *roaM* or *ompB* at 65°C for 5 min and chilled on ice for 2 min. Then, 0.5 mM concentrations of deoxynucleoside triphosphates (dNTPs), 5 mM dithiothreitol (DTT), 100 U SuperScript IV, and 1× SuperScript IV buffer were added, and the reaction mixture was incubated at 50°C for 60 min. Template switching oligomer (TSO; 1 μM; ANP0451), an additional 100 U SuperScript IV, 1× SuperScript IV buffer, and 5 mM DTT were added. Next, 2 mM $MnCl_2$, 2 mM $MgCl_2$, and 0.1% BSA (NEB, B9000S) were included to increase the efficiency of the addition of cytosine residues by the reverse transcriptase upon interaction with the cap structure (71), and the reaction mixture was incubated at 42°C for 90 min. Two units of *E. coli* RNase H was added, and the reaction mixture was incubated for 20 min at 37°C to remove RNA. The reaction mixture was then used for nested PCR with *Taq* DNA polymerase (NEB, M0273) using primers ANP0452 and ANP0453 with gene specific primers. PCR products were then cloned into pGEM-T Easy (Promega, A1360) for sequencing.

Serial passage experiment. Plaque-purified *R. rickettsii* SS_5 was used to infect Vero 76 cells in three T25 flasks to initiate three different lineages. Each flask was harvested on Tuesdays and Fridays (alternating 3- and 4-day incubations) by scraping the host cell monolayer into 1 mL of BHI and disrupted for 10 s with glass beads. One hundred microliters of supernatant was used to inoculate the next T25 flask of Vero 76 cells, and the remainder was frozen. Even-numbered passages were plaqued at several dilutions and stained with MTT after 10 days of incubation at 34°C. At passage 10, a single large plaque from each lineage was plaque cloned twice and used for DNA isolation. The *roaM* region was amplified (primers ANP0212 and ANP0276) and Sanger sequenced.

Guinea pig fever curves. Female Hartley guinea pigs (300 to 500 g; 5 to 8 weeks of age) (Charles River Laboratories) were obtained and housed in compliance with a protocol (2017-064.2) approved by the Rocky Mountain Laboratories Animal Care and Use committee. To monitor temperatures, transponders (Bio Medic Data Systems, Inc., Seaford, DE) were implanted subcutaneously. One hundred PFU was delivered via intradermal injection, and temperature was recorded daily for 16 days postinfection. At 28 days postinfection, sera were collected for antibody titration and animals were euthanized.

SUPPLEMENTAL MATERIAL

Supplemental material is available online only.

FIG S1, TIF file, 0.3 MB.

FIG S2, TIF file, 0.4 MB.

FIG S3, TIF file, 0.4 MB.

FIG S4, TIF file, 0.3 MB.

TABLE S1, DOCX file, 0.02 MB.

TABLE S2, DOCX file, 0.01 MB.

TABLE S3, DOCX file, 0.02 MB.

ACKNOWLEDGMENTS

This work was supported by the Intramural Research Program of the NIAID/NIH.

We thank Ulrike Munderloh for the gift of pRAM18dSFA[MCS] (Addgene plasmid 84685). We thank C. Paddock and K. Macaluso for review of the manuscript and their constructive comments. We also thank T. Schwan for critical reading of the manuscript. The assistance of Jacqueline Leung in microscopy protocols is gratefully acknowledged.

REFERENCES

1. Ricketts HT. 1991. Some aspects of Rocky Mountain spotted fever as shown by recent investigations. 1909. Rev Infect Dis 13:1227–1240. https://doi.org/10.1093/clinids/13.6.1227.
2. Wolbach SB. 1919. Studies on Rocky Mountain spotted fever. J Med Res 41:1–198.141.
3. Hattwick MAW. 1971. Rocky mountain spotted fever in the United States, 1920–1970. JInfectDis 124:112–114. https://doi.org/10.1093/infdis/124.1.112.
4. Walker DH. 1989. Rocky Mountain spotted fever: a disease in need of microbiological concern. Clin Microbiol Rev 2:227–240. https://doi.org/10.1128/CMR.2.3.227.
5. Álvarez-Hernández G, Roldán JFG, Milan NSH, Lash RR, Behravesh CB, Paddock CD. 2017. Rocky Mountain spotted fever in Mexico: past, present, and future. Lancet Infect Dis 17:e189–e196. https://doi.org/10.1016/S1473-3099(17)30173-1.
6. Heitman KN, Drexler NA, Cherry-Brown D, Peterson AE, Armstrong PA, Kersh GJ. 2019. National surveillance data show increase in spotted fever rickettsiosis: United States, 2016–2017. Am J Public Health 109:719–721. https://doi.org/10.2105/AJPH.2019.305038.
7. Sonenshine DE. 2018. Range expansion of tick disease vectors in North America: implications for spread of tick-borne disease. Int J Environ Res Public Health 15:478. https://doi.org/10.3390/ijerph15030478.
8. Heinzen RA, Hayes SF, Peacock MG, Hackstadt T. 1993. Directional actin polymerization associated with spotted fever group rickettsia infection of VERO cells. Infect Immun 61:1926–1935. https://doi.org/10.1128/iai.61.5.1926-1935.1993.
9. Teysseire N, Chiche-Portiche C, Raoult D. 1992. Intracellular movements of *Rickettsia conorii* and *R. typhi* based on actin polymerization. Res Microbiol 143:821–829. https://doi.org/10.1016/0923-2508(92)90069-Z.
10. Tilney LG, Portnoy DA. 1989. Actin filaments and the growth, movement, and spread of the intracellular bacterial parasite, *Listeria monocytogenes*. J Cell Biol 109:1597–1608. https://doi.org/10.1083/jcb.109.4.1597.
11. Bernardini ML, Mounier J, d'Hauteville H, Coquis-Rondon M, Sansonetti PJ. 1989. Identification of *icsA*, a plasmid locus of *Shigella flexneri* that governs bacterial intra- and intercellular spread through interaction with F-actin. Proc Natl Acad Sci U S A 86:3867–3871. https://doi.org/10.1073/pnas.86.10.3867.
12. Kespichayawattana W, Rattanachetkul S, Wanun T, Utaisincharoen P, Sirisinha S. 2000. *Burkholderia pseudomallei* induces cell fusion and actin-associated membrane protrusion: a possible mechanism for cell-to-cell spreading. Infect Immun 68:5377–5384. https://doi.org/10.1128/IAI.68.9.5377-5384.2000.
13. Kocks C, Gouin E, Tabouret M, Berche P, Ohayon H, Cossart P. 1992. *L. monocytogenes*-induced actin assembly requires the *actA* gene product, a surface protein. Cell 68:521–531. https://doi.org/10.1016/0092-8674(92)90188-I.
14. Sun AN, Camilli A, Portnoy DA. 1990. Isolation of *Listeria monocytogenes* small-plaque mutants defective for intracellular growth and cell-to-cell spread. Infect Immun 58:3770–3778. https://doi.org/10.1128/iai.58.11.3770-3778.1990.
15. Stevens JM, Galyov EE, Stevens MP. 2006. Actin-dependent movement of bacterial pathogens. Nat Rev Microbiol 4:91–101. https://doi.org/10.1038/nrmicro1320.
16. Kordová N. 1966. Plaque assay of rickettsiae. Acta Virol 10:278.
17. Weinberg EH, Stakebake JR, Gerone PJ. 1969. Plaque assay for *Rickettsia rickettsii*. J Bacteriol 98:398–402. https://doi.org/10.1128/jb.98.2.398-402.1969.
18. McDade JE, Stakebake JR, Gerone PJ. 1969. Plaque assay system for several species of *Rickettsia*. J Bacteriol 99:910–912. https://doi.org/10.1128/jb.99.3.910-912.1969.
19. Cory J, Yunker CE, Ormsbee RA, Peacock M, Meibos H, Tallent G. 1974. Plaque assay of rickettsiae in a mammalian cell line. Appl Microbiol 27:1157–1161. https://doi.org/10.1128/am.27.6.1157-1161.1974.
20. Kleba B, Clark TR, Lutter EI, Ellison DW, Hackstadt T. 2010. Disruption of the *Rickettsia rickettsii* Sca2 autotransporter inhibits actin-based motility. Infect Immun 78:2240–2247. https://doi.org/10.1128/IAI.00100-10.
21. Clark TR, Ellison DW, Kleba B, Hackstadt T. 2011. Complementation of *Rickettsia rickettsii* RelA/SpoT restores a nonlytic plaque phenotype. Infect Immun 79:1631–1637. https://doi.org/10.1128/IAI.00048-11.
22. Lamason RL, Kafai NM, Welch MD. 2018. A streamlined method for transposon mutagenesis of *Rickettsia parkeri* yields numerous mutations that impact infection. PLoS One 13:e0197012. https://doi.org/10.1371/journal.pone.0197012.
23. Haglund CM, Choe JE, Skau CT, Kovar DR, Welch MD. 2010. Rickettsia Sca2 is a bacterial formin-like mediator of actin-based motility. Nat Cell Biol 12:1057–1063. https://doi.org/10.1038/ncb2109.
24. Noriea NF, Clark TR, Mead D, Hackstadt T. 2017. Proteolytic cleavage of the immunodominant outer membrane protein rOmpA in *Rickettsia rickettsii*. J Bacteriol 199:e00826-16. https://doi.org/10.1128/JB.00826-16.
25. Ellison DW, Clark TR, Sturdevant DE, Virtaneva K, Porcella SF, Hackstadt T. 2008. Genomic comparison of virulent *Rickettsia rickettsii* Shiela Smith and avirulent *Rickesttia rickettsii* Iowa. Infect Immun 76:542–550. https://doi.org/10.1128/IAI.00952-07.
26. Clark TR, Noriea NF, Bublitz DC, Ellison DW, Martens C, Lutter EI, Hackstadt T. 2015. Comparative genome sequencing of *Rickettsia rickettsii* strains that differ in virulence. Infect Immun 83:1568–1576. https://doi.org/10.1128/IAI.03140-14.
27. Hackstadt T, Messer R, Cieplak W, Peacock MG. 1992. Evidence for the proteolytic cleavage of the 120-kilodalton outer membrane protein of rickettsiae: identification of an avirulent mutant deficient in processing. Infect Immun 60:159–165. https://doi.org/10.1128/iai.60.1.159-165.1992.
28. Liu F, Zheng K, Chen HC, Liu ZF. 2018. Capping-RACE: a simple, accurate, and sensitive 5' RACE method for use in prokaryotes. Nucleic Acids Res 46:e129.
29. Taboada B, Ciria R, Martinez-Guerrero CE, Merino E. 2012. ProOpDB: Prokaryotic Operon DataBase. Nucleic Acids Res 40:D627–D631. https://doi.org/10.1093/nar/gkr1020.
30. Lehman SS, Noriea NF, Aistleitner K, Clark TR, Dooley CA, Nair V, Kaur SJ, Rahman MS, Gillespie JJ, Azad AF, Hackstadt T. 2018. The rickettsial ankyrin repeat protein 2 is a type IV secreted effector that associates with the endoplasmic reticulum. mBio 9:e00975-18. https://doi.org/10.1128/mBio.00975-18.
31. Gouin E, Egile C, Dehoux P, Villiers V, Adams J, Gertler F, Li R, Cossart P. 2004. The RickA protein of *Rickettsia conorii* activates the Arp2/3 complex. Nature 427:457–461. https://doi.org/10.1038/nature02318.
32. Jeng RL, Goley ED, D'Alessio JA, Chaga OY, Svitkina TM, Borisy GG, Heinzen RA, Welch MD. 2004. A Rickettsia WASP-like protein activates the Arp2/3 complex and mediates actin-based motility. Cell Microbiol 6:761–769. https://doi.org/10.1111/j.1462-5822.2004.00402.x.
33. Lamason RL, Bastounis E, Kafai NM, Serrano R, Del Álamo JC, Theriot JA, Welch MD. 2016. Rickettsia Sca4 reduces vinculin-mediated intercellular tension to promote spread. Cell 167:670–683.E610. https://doi.org/10.1016/j.cell.2016.09.023.
34. Davis JJ, Wattam AR, Aziz RK, Brettin T, Butler R, Butler RM, Chlenski P, Conrad N, Dickerman A, Dietrich EM, Gabbard JL, Gerdes S, Guard A, Kenyon RW, Machi D, Mao C, Murphy-Olson D, Nguyen M, Nordberg EK, Olsen GJ, Olson RD, Overbeek JC, Overbeek R, Parrello B, Pusch GD, Shukla M, Thomas C, VanOeffelen M, Vonstein V, Warren AS, Xia F, Xie D, Yoo H, Stevens R. 2020. The PATRIC Bioinformatics Resource Center: expanding data and analysis capabilities. Nucleic Acids Res 48:D606–D612.
35. Duan C, Tong Y, Huang Y, Wang X, Xiong X, Wen B. 2011. Complete genome sequence of *Rickettsia heilongjiangensis*, an emerging tick-transmitted human pathogen. J Bacteriol 193:5564–5565. https://doi.org/10.1128/JB.05852-11.
36. Kasama K, Fujita H, Yamamoto S, Ooka T, Gotoh Y, Ogura Y, Ando S, Hayashi T. 2019. Genomic features of *Rickettsia heilongjiangensis* revealed by intraspecies comparison and detailed comparison with *Rickettsia japonica*. Front Microbiol 10:2787. https://doi.org/10.3389/fmicb.2019.02787.
37. Diop A, Raoult D, Fournier PE. 2018. Rickettsial genomics and the paradigm of genome reduction associated with increased virulence. Microbes Infect 20:401–409. https://doi.org/10.1016/j.micinf.2017.11.009.
38. Diard M, Hardt WD. 2017. Evolution of bacterial virulence. FEMS Microbiol Rev 41:679–697. https://doi.org/10.1093/femsre/fux023.
39. Duangurai T, Reamtong O, Rungruengkitkun A, Srinon V, Boonyuen U, Limmathurotsakul D, Chantratita N, Pumirat P. 2020. In vitro passage alters virulence, immune activation and proteomic profiles of Burkholderia pseudomallei. Sci Rep 10:8320. https://doi.org/10.1038/s41598-020-64914-4.
40. Domenech P, Reed MB. 2009. Rapid and spontaneous loss of phthiocerol dimycocerosate (PDIM) from *Mycobacterium tuberculosis* grown in vitro: implications for virulence studies. Microbiology (Reading) 155:3532–3543. https://doi.org/10.1099/mic.0.029199-0.
41. Beare PA, Jeffrey BM, Long CM, Martens CM, Heinzen RA. 2018. Genetic mechanisms of *Coxiella burnetii* lipopolysaccharide phase variation. PLoS Pathog 14:e1006922. https://doi.org/10.1371/journal.ppat.1006922.
42. Fiset P. 1957. Phase variation of *Rickettsia (Coxiella) burneti*; study of the antibody response in guinea pigs and rabbits. Can J Microbiol 3:435–445. https://doi.org/10.1139/m57-046.

43. Makela PH, Mayer H. 1976. Enterobacterial common antigen. Bacteriol Rev 40:591–632. https://doi.org/10.1128/br.40.3.591-632.1976.
44. Cox HR. 1941. Cultivation of *Rickettsiae* of the Rocky Mountain spotted fever, typhus and Q fever groups in the embryonic tissues of developing chicks. Science 94:399–403. https://doi.org/10.1126/science.94.2444.399.
45. Noriea NF, Clark TR, Hackstadt T. 2015. Targeted knockout of the *Rickettsia rickettsii* OmpA surface antigen does not diminish virulence in a mammalian model system. mBio 6:e00323-15. https://doi.org/10.1128/mBio.00323-15.
46. Baldridge GD, Burkhardt NY, Simser JA, Kurtti TJ, Munderloh UG. 2004. Sequence and expression analysis of the *ompA* gene of *Rickettsia peacockii*, an endosymbiont of the Rocky Mountain wood tick, *Dermacentor andersoni*. Appl Environ Microbiol 70:6628–6636. https://doi.org/10.1128/AEM.70.11.6628-6636.2004.
47. Felsheim RF, Kurtti TJ, Munderloh UG. 2009. Genome sequence of the endosymbiont *Rickettsia peacockii* and comparison with virulent *Rickettsia rickettsii*: identification of virulence factors. PLoS One 4:e8361. https://doi.org/10.1371/journal.pone.0008361.
48. Burgdorfer W. 1963. Investigation of "transovarial transmission" of *Rickettsia rickettsii* in the wood tick, *Dermacentor andersoni*. Exp Parasitol 14:152–159. https://doi.org/10.1016/0014-4894(63)90019-5.
49. Niebylski ML, Peacock MG, Schwan TG. 1999. Lethal effect of *Rickettsia rickettsii* on its tick vector (*Dermacentor andersoni*). Appl Environ Microbiol 65:773–778. https://doi.org/10.1128/AEM.65.2.773-778.1999.
50. Labruna MB, Ogrzewalska M, Soares JF, Martins TF, Soares HS, Moraes-Filho J, Nieri-Bastos FA, Almeida AP, Pinter A. 2011. Experimental infection of *Amblyomma aureolatum* ticks with *Rickettsia rickettsii*. Emerg Infect Dis 17:829–834. https://doi.org/10.3201/eid1705.101524.
51. Schumacher L, Snellgrove A, Levin ML. 2016. Effect of *Rickettsia rickettsii* (Rickettsiales: Rickettsiaceae) infection on the biological parameters and survival of its tick vector-*Dermacentor variabilis* (Acari: Ixodidae). J Med Entomol 53:172–176. https://doi.org/10.1093/jme/tjv166.
52. Piranda EM, Faccini JL, Pinter A, Pacheco RC, Cançado PH, Labruna MB. 2011. Experimental infection of *Rhipicephalus sanguineus* ticks with the bacterium *Rickettsia rickettsii*, using experimentally infected dogs. Vector Borne Zoonotic Dis 11:29–36. https://doi.org/10.1089/vbz.2009.0250.
53. Freitas LH, Faccini JL, Labruna MB. 2009. Experimental infection of the rabbit tick, *Haemaphysalis leporispalustris*, with the bacterium *Rickettsia rickettsii*, and comparative biology of infected and uninfected tick lineages. Exp Appl Acarol 47:321–345. https://doi.org/10.1007/s10493-008-9220-4.
54. Macaluso KR, Sonenshine DE, Ceraul SM, Azad AF. 2001. Infection and transovarial transmission of rickettsiae in *Dermacentor variabilis* ticks acquired by artificial feeding. Vector Borne Zoonotic Dis 1:45–53. https://doi.org/10.1089/153036601750137660.
55. Niebylski ML, Schrumpf ME, Burgdorfer W, Fischer ER, Gage KL, Schwan TG. 1997. *Rickettsia peacockii* sp. nov., a new species infecting wood ticks, *Dermacentor andersoni*, in western Montana. Int J Syst Bacteriol 47:446–452. https://doi.org/10.1099/00207713-47-2-446.
56. Simser JA, Palmer AT, Munderloh UG, Kurtti TJ. 2001. Isolation of a spotted fever group rickettsia, *Rickettsia peacockii*, in a Rocky Mountain wood tick, *Dermacentor andersoni*, cell line. Appl Environ Microbiol 67:546–552. https://doi.org/10.1128/AEM.67.2.546-552.2001.
57. Price WH. 1954. Variation in virulence of "Rickettsia rickettsii" under natural and experimental conditions, p 164–183. *In* Hartman FW, Horsfall FL, Kidd JG (ed), The dynamics of virus and rickettsial infections. The Blakiston Co., Inc., New York, NY.
58. Cooper VS. 2018. Experimental evolution as a high-throughput screen for genetic adaptations. mSphere 3:e00121-18. https://doi.org/10.1128/mSphere.00121-18.
59. Sakamoto JM, Azad AF. 2007. Propagation of arthropod-borne *Rickettsia* spp. in two mosquito cell lines. Appl Environ Microbiol 73:6637–6643. https://doi.org/10.1128/AEM.00923-07.
60. Kelley LA, Mezulis S, Yates CM, Wass MN, Sternberg MJ. 2015. The Phyre2 web portal for protein modeling, prediction and analysis. Nat Protoc 10:845–858. https://doi.org/10.1038/nprot.2015.053.
61. Coordinators NR. 2018. Database resources of the National Center for Biotechnology Information. Nucleic Acids Res 46:D8–D13. https://doi.org/10.1093/nar/gkx1095.
62. Greenberg MJ, Arpağ G, Tüzel E, Ostap EM. 2016. A perspective on the role of myosins as mechanosensors. Biophys J 110:2568–2576. https://doi.org/10.1016/j.bpj.2016.05.021.
63. Mueller KE, Wolf K, Fields KA. 2016. Gene deletion by fluorescence-reported allelic exchange mutagenesis in *Chlamydia trachomatis*. mBio 7:e01817-15. https://doi.org/10.1128/mBio.01817-15.
64. Laemmli UK. 1970. Cleavage of structural proteins during the assembly of the head of bacteriophage T4. Nature 227:680–685. https://doi.org/10.1038/227680a0.
65. Towbin H, Staehelin T, Gordon J. 1979. Electrophoretic transfer of proteins from polyacrylamide gels to nitrocellulose sheets: procedure and some applications. Proc Natl Acad Sci U S A 76:4350–4354. https://doi.org/10.1073/pnas.76.9.4350.
66. Anacker RL, Mann RE, Gonzales C. 1987. Reactivity of monoclonal antibodies to *Rickettsia rickettsii* with spotted fever and typhus group rickettsiae. J Clin Microbiol 25:167–171. https://doi.org/10.1128/jcm.25.1.167-171.1987.
67. Schindelin J, Arganda-Carreras I, Frise E, Kaynig V, Longair M, Pietzsch T, Preibisch S, Rueden C, Saalfeld S, Schmid B, Tinevez JY, White DJ, Hartenstein V, Eliceiri K, Tomancak P, Cardona A. 2012. Fiji: an open-source platform for biological-image analysis. Nat Methods 9:676–682. https://doi.org/10.1038/nmeth.2019.
68. Otsu N. 1979. A threshold selection method from gray-level histograms. IEEE Trans Syst Man Cybern 9:62–66. https://doi.org/10.1109/TSMC.1979.4310076.
69. Livak KJ, Schmittgen TD. 2001. Analysis of relative gene expression data using real-time quantitative PCR and the $2^{-\Delta\Delta CT}$ method. Methods 25:402–408. https://doi.org/10.1006/meth.2001.1262.
70. de Witt J, Oetermann S, Parise M, Parise D, Baumbach J, Steinbüchel A. 2020. Global regulator of rubber degradation in *Gordonia polyisoprenivorans* VH2: identification and involvement in the regulation network. Appl Environ Microbiol 86:e00773-20. https://doi.org/10.1128/AEM.00774-20.
71. Schmidt WM, Mueller MW. 1999. CapSelect: a highly sensitive method for 5' CAP-dependent enrichment of full-length cDNA in PCR-mediated analysis of mRNAs. Nucleic Acids Res 27:e31.